A Thin, Low-Profile Antenna Using a Novel High Impedance Ground Plane

Introduction

The size of the antenna for a given application does not depend purely on the technology but on the laws of physics where the antenna size with respect to the wavelength has the predominant influence on the radiation characteristics. With modern day communication devices becoming smaller and lighter, demand for low-profile antenna designs is greater than ever [1]. One way of realizing a low-profile antenna design is to use a high impedance ground plane in place of the conventional metallic ground plane [2-7]. Metallic plates are used as ground planes to redirect the back radiation and provide shielding to the antennas. By nature, the conventional ground planes that are perfect electric conductors (PECs) exhibit the property of phase reversal of the incident currents that result in destructive interference of the original antenna currents and the image currents. To overcome this effect, antennas are to be placed at a height of quarter wavelength above the metallic ground plane making the size of the antenna bulky at low frequencies. To reduce the size of the antenna, we need a ground plane that is dual of the conventional PECs, in other words we need a PMC (perfect magnetic conductor). How can we realize a PMC that is not available in nature? The answer to this problem is provided in the form of high impedance surfaces (HISs) which can essentially be considered as artificial magnetic conductors [8, 9]. HISs are popular for their wide-spread applications in reflect array antennas, low-profile antennas, electromagnetic absorbers and polarizers [10-13]. These surfaces exhibit unique properties like the in-phase reflection of incident waves and the suppression of the surface waves. Different antenna parameters like the gain, impedance and the size can be enhanced by incorporating the HISs into the antenna structures. The design of the HISs can be optimized to tailor their electromagnetic properties depending on the operational requirements. Computer aided design tools have enabled the solution of complex problems by means of numerical optimization algorithms [14, 15]. A large number of optimization methods are presently available for solving electromagnetic problems. Deciding the most appropriate method for a given problem however is a non-trivial task and depends on the factors like the number and range of the varying parameters, the goal of the optimization, the model size and the resources available.

The two-dimensional (2D) arrays of periodic resonant elements (printed or complimentary slot) interact with electromagnetic waves within certain frequency band(s) and can be characterized as frequency selective surfaces (FSSs). Figure 1, 2, and 3 show different FSS elements from the literature where each design has its own advantage over the other.

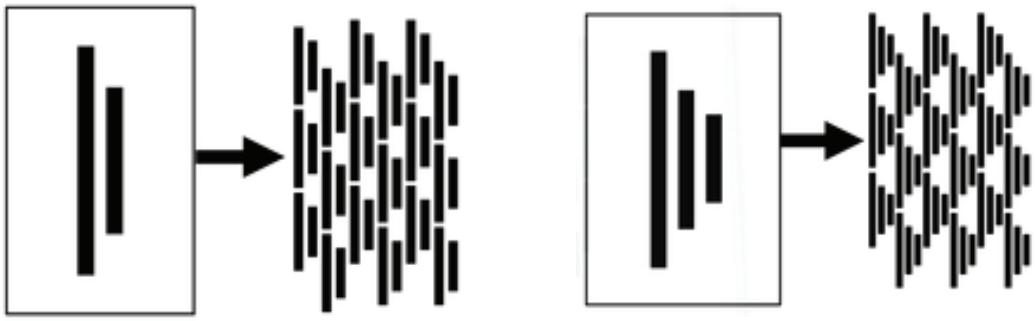

(a) Dual band *(b) Triple band*

Figure 1: Multiband perturbed FSS structures [16]

(a) Rectangular loop *(b) Circular loop* *(c) Jerusalem cross* *(d) Rectangular patch*

Figure 2: Dual-polarized FSS elements

(a) Tripole *(b) Rectangular patch*

Figure 3: Fractal FSS elements

The multiband dipole structures are polarization dependent, the symmetric designs are dual-polarized and the fractal structures are compact designs. The HIS is realized by printing the periodic array of FSSs over a metal backed dielectric substrate. It is important to optimize the performance of HIS over the frequencies of interest. It is observed that the characteristics of the FSS and HIS follow each other and this correlation can be exploited to speed up the optimization process by carrying out the design in two steps:

1. Optimize the free-standing FSS
2. Realize the HIS by printing the optimized FSS on a metal backed dielectric substrate

Even though there is growing demand for wideband antennas, a narrowband design has its advantages in cordless and wireless phone applications that operate at 49 MHz, 900 MHz, 2.4 GHz and 5.8 GHz. Interference from adjacent frequency bands can be avoided by using narrowband antennas that operate only around the frequency of interest. This article describes a novel FSS structure that is optimized for steep behavior of the reflection coefficient. The FSS unit cell is the combination of the Jerusalem cross and the three step fractal patch as shown in Figure 4.

(a) Unit cell *(b) FSS structure*

Figure 4: Combination of Jerusalem cross and three-step fractal patch

The reflection characteristics of the FSS structure are explored in designing a HIS that can be used as a potential substrate for antennas in cordless phone applications to reduce cross talk. The performance of the HIS substrate is demonstrated with a 5.8 GHz low-profile monopole (quarter wavelength) antenna with a 0.07 λ dielectric thickness. The monopole is first analyzed as a wire structure and then this design is translated to a printed format.

FSS Design and Optimization

The operation of the FSS structure depends on the resonance of the unit cell. The periodic array of the unit cell interacts with the electromagnetic wave and resonates at certain frequencies where it acts as a band stop filter with total reflection of the incident plane wave as shown in Figure 5.

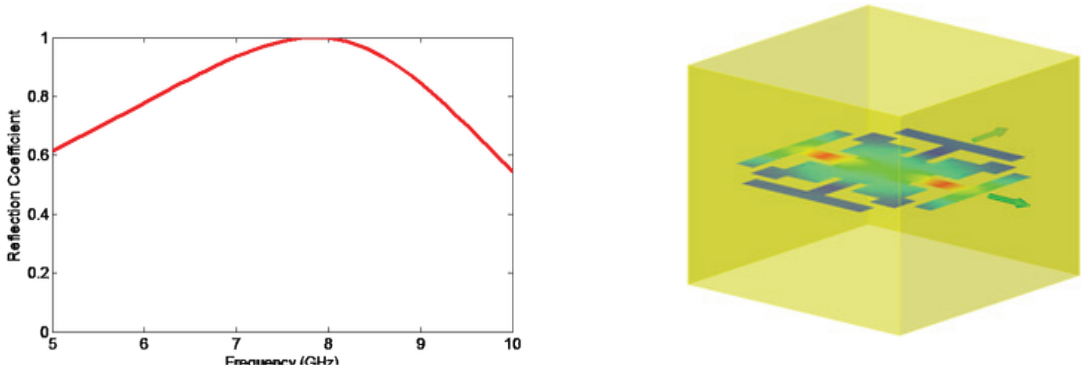

(a) Reflectivity behaviour *(b) Current distribution on the unit cell*

Figure 5: Performance characterization of the proposed FSS

The initial design of the FSS structure with broad band characteristics is optimized for sharp narrow band characteristics. Commercial software FEKO [22] is used for the analysis of the FSS structure using two different optimization methods: simplex Nelder-Mead and the particle swarm optimization (PSO) [20].

Simplex (Nelder-Mead Method)

The simplex Nelder-Mead algorithm is a local or hill climbing algorithm in which the final optimum relies strongly on the starting point. The term simplex refers to the geometric figure formed by a set of N+1 points in an N-dimensional space. The basic idea of the simplex method is the comparison of values of the combined optimization goals at the N+1 points of the general simplex (where each point represents a single set of parameter values) to facilitate the movement of the simplex towards the optimum point during an iterative process. The movement of the simplex is achieved using three operations: reflection, expansion, and contraction.

Particle Swarm Optimization (PSO)

Particle swarm optimization is a global search algorithm which is a population based stochastic evolutionary computation technique based on the movement and intelligence of swarms found in nature. The mechanism of PSO can be best described using the analogy of a swarm of bees in a field whose goal is to find the highest concentration of flowers where each bee represents a set of parameter values. Every bee has information about the position of flower abundance based on its own experience (local best) and the position of maximum flower abundance based on the experience of all the other bees (global best). Based on the weights given to individuality or peer pressure a bee flies in a direction, between the positions of the local and the global bests. Once the flying is done, the bee conveys the new found information to all the other bees which then adjust their positions and velocities. With this constant exploring and exchange of information, all the bees are eventually drawn towards the position of highest concentration of flowers.

The possible optimization parameters/variables in the proposed FSS unit cell are the dimensions of the Jerusalem cross arms and the fractal patch. An optimization mask was used to specify the optimization goal as shown in Figure 6.

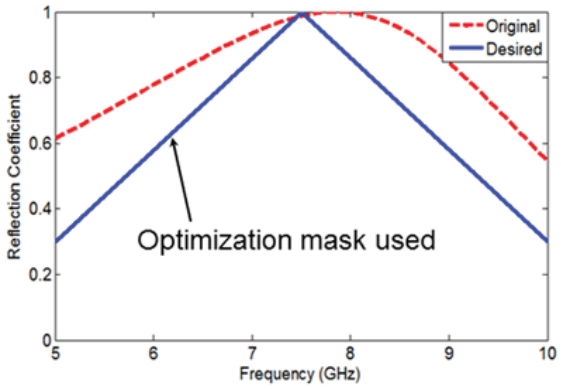

Figure 6: FSS reflectivity behaviour, original and the desired (goal of optimization)

Being a local optimizer, the convergence of the simplex algorithm is much faster compared to the global optimizer PSO. But, unlike the global optimizer PSO, the success of the simplex depends on the starting point that carries the disadvantage of converging at a local minimum. From Figure 7, it is clear that the global optimizer PSO was able to approximate the mask more closely compared to the simplex but at the cost of huge runtime (see Table-1 for runtimes).

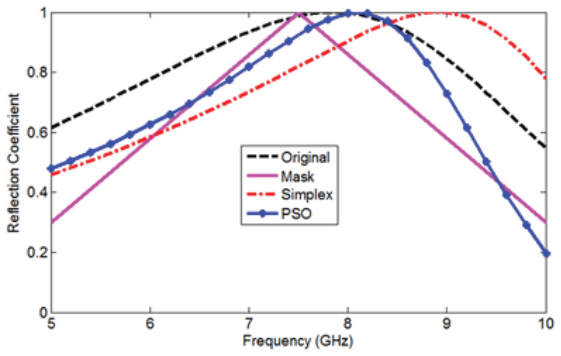

Figure 7: Comparison of the simple and PSO algorithms

To improve the chances of reaching the global minimum without compromising on the speed of convergence, PSO is hybridized with simplex where the global optimizer will be used to find the starting point for the local optimizer. The hybridized method has improved the speed of the optimizer without compromising on the ability to reach the global goal. In this process the local optimizer was started after 100 iterations of the global optimizer. The local optimizer simplex converged to the global minimum in 154 iterations as shown in Figure 8, reducing the runtime by 95%.

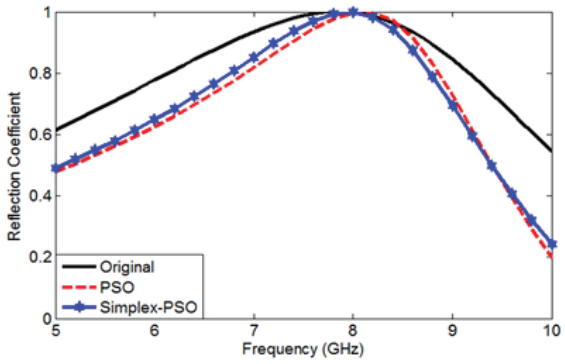

Figure 8: Comparison between PSO and Simplex-PSO hybrid optimization

Table-1, describes the number of iterations and the time taken for each optimization algorithm to converge on a 2 GHz, EM64T Linux machine that has 2 physical CPUs with 4 cores per CPU.

Optimization algorithm	No. of iterations	Time taken (hours)
PSO	5000	900
Simplex	179	32.2
Nelder-Mead	254	45.7

Table 1: Optimization performance

HIS Design and Validation

The optimization completes the first step in the realization of artificial magnetic conductor taking the design process to the next stage where the optimized FSS structure shown in Figure 9(b) is printed on a metal backed dielectric substrate. The design parameters of the HIS shown in Figure 10 are given in Table-2, where λ_d denotes the wavelength inside the dielectric at 5.8 GHz.

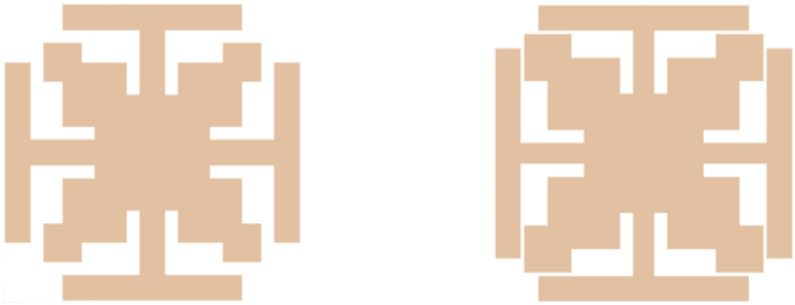

(a) Initial unit cell *(b) Optimized unit cell*

Figure 9: FSS unit cell geometry

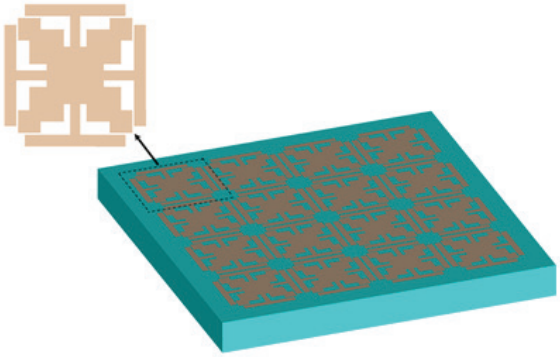

Figure 10: HIS realized with optimized FSS

Periodicity of the unit cell	7.6 mm
Dielectric constant of the substrate	$\varepsilon_r = 2.2$
Nelder-Mead	3 mm = 0.07 λ_d

Table 2: HIS design parameters

The reflectivity characteristics of the HIS ground planes realized using the un-optimized and the optimized FSS structures reveals the correlation between the FSS and the HIS. The HIS realized with optimized FSS reduced the bandwidth of the un-optimized design by 7% as shown Figure 11, where the bandwidth is defined for the phase of the reflection coefficient varying between +90 and -90 degrees.

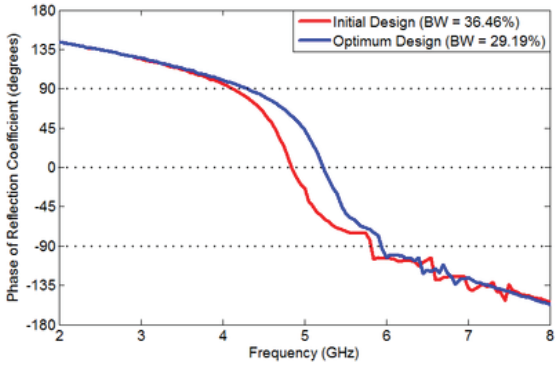

Figure 11: Reflectivity characteristics of HIS realized with un-optimized and optimized FSS

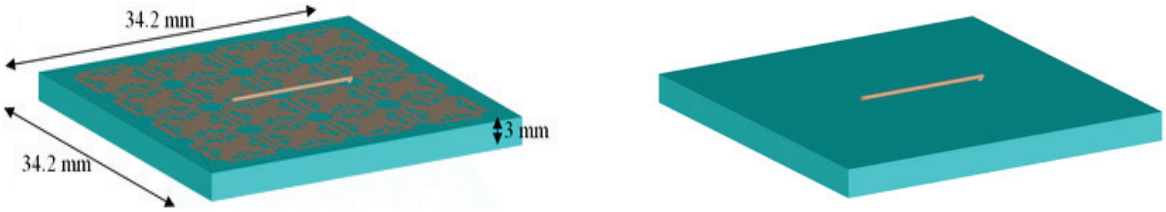

(a) Monopole antenna on HIS groundplane *(b) Monopole on metal backed dielectric substrate*

Figure 12: Design comparisonstch

Figure 13 validates the performance of the HIS ground plane with low return loss and an improvement of 7.5 dB in the gain over the metal backed dielectric substrate.

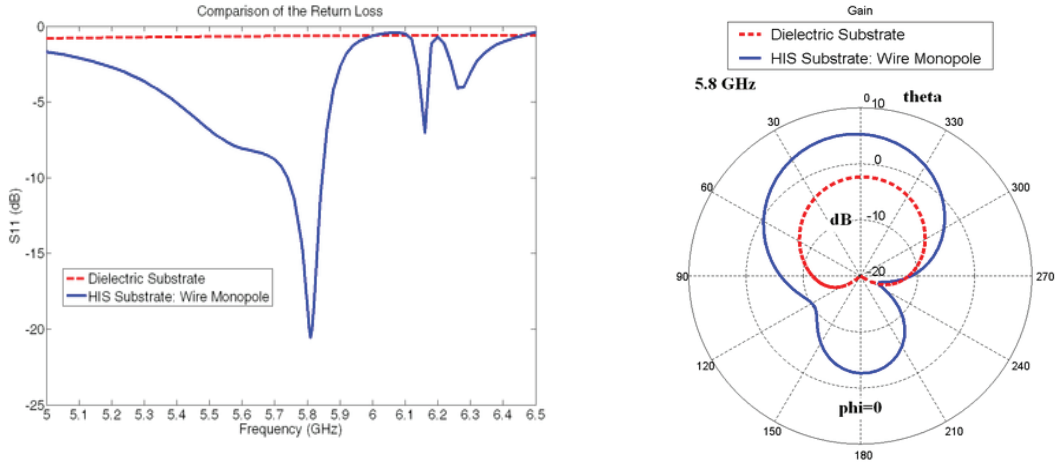

(a) Return loss of monopole *(b) Monopole antenna gain*

Figure 13: Antenna performance at 5.8 GHz (Elevation phi=0) on HIS and dielectric substrates

Planar Antenna

Antennas are generally preferred in a printed format so that they can be made flush with the surrounding environment. Printed planar antennas also have the advantage of being cheap and more convenient to manufacture and lend themselves more easily to mass production than non-printed antennas. For these reasons we transfer our design from the protruding cylindrical monopole structure to one involving a planar printed monopole.

The wire monopole (modeled as a cylinder) is transformed to the printed monopole using the well known formula , where ‘a’ is the radius of the cylinder and ‘w’ is the width of the strip. This strip monopole is located at the same height as the axis of the cylindrical monopole to keep the electromagnetic relationship between the high impedance surface (HIS) and the monopole intact. It is not desirable that the gap between the strip monopole and the top surface be left as free-space as this leaves the monopole vulnerable to damage and also defeats the purpose of ease of manufacture. In order to avoid these problems we fill this space with a dielectric superstrate (relative to the HIS) that has the same dielectric properties as the substrate. Figure 14(a) shows the printed monopole antenna on top of the newly added dielectric layer. The HIS is located at the boundary of the dielectric layers and can be seen in the wire frame view. Figure 14(b) displays the coaxial cable feeding mechanism in a cut-plane view. A TEM mode is excited from an end of the cable whose outer conductor terminates at the ground plane and inner conductor extends further through the substrate to excite one end of the monopole.

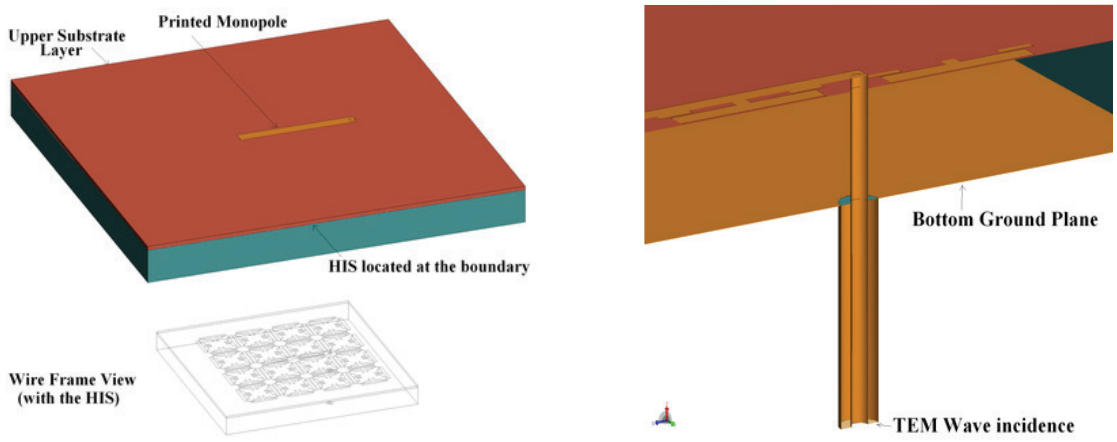

(a) HIS groundplane between substrate layers *(b) Co-axial feed for the monopole*

Figure 14: Geometry of a printed monopole antenna with HIS groundplane

Replacing the air layer with a dielectric substrate alters the electrical length of both the monopole and the HIS, thereby moving the resonant frequency away from the desired value of 5.8 GHz. To re-tune the antenna back to 5.8 GHz we scale the monopole by a factor

$$\frac{1}{\sqrt{(\varepsilon_r + 1)/2}}$$

of and the HIS by a factor of

$$\sqrt{\left(\frac{\varepsilon_r + 1}{2}\right)/\varepsilon_r}$$

It should be pointed out that although the scaling brings the resonance very close to 5.8 GHz; some finer adjustments of these factors is required to make the resonance fall exactly at 5.8 GHz. Figure 15 compares the S_{11} of the planar design with the previous non-planar design and the non-HIS substrate. From the graph we note that the planar design leads to an increase in the return loss bandwidth (defined as being lower than 10dB). Due to the improved impedance match at our center frequency we find that the gain of the antenna is increased from a value of 5.35 dB (non-planar monopole) to a value of 7.73 dB (planar monopole). Figure 16 illustrates this behavior and shows the gain pattern in the elevation plane (XZ).

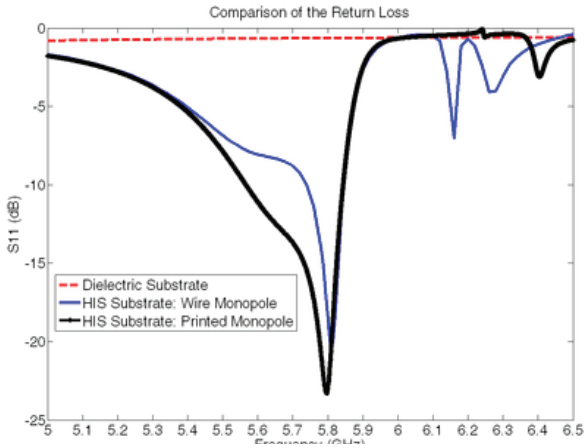

Figure 15: Comparison of return loss for printed monopole antenna

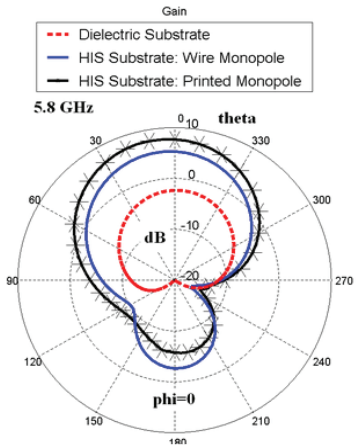

Figure 16: Monopole antenna gain for the planar and non-planar antennas at 5.8 GHz

Effect of the Substrate Length and Width

As overall size of the antenna including the HIS ground plane is important for use in compact mobile devices, we also studied the effect of substrate length and width on the impedance characteristics of the antenna. Figure 17 shows the variation in return loss due to decrease in substrate size. It can be seen that decrease in substrate size narrows the impedance bandwidth. Substrate size can be used to control the impedance bandwidth..

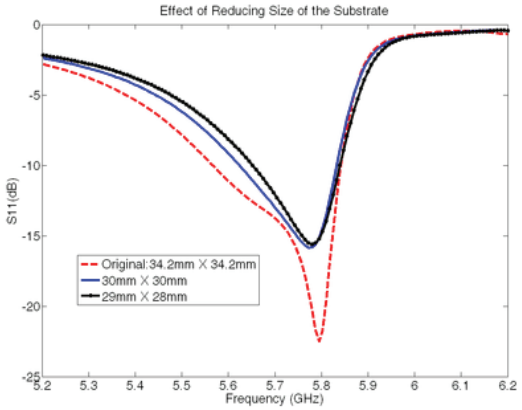

Figure 17: Effect of the substrate size

Conclusion

A novel FSS structure is designed by combining the fractal and the Jerusalem cross elements. The resultant structure provides more flexibility in controlling the reflection coefficient behavior. The efficiency of the optimizers can be increased by hybridizing the local optimizer with the global optimizer, which is demonstrated in the case of the proposed FSS structure. The narrowband HIS realized from the optimized FSS can be used in designing low-profile antennas. The low-profile monopole antenna on the HIS ground plane with a substrate thickness of 0.07 λ_d improves the gain of the antenna by 7.5 dB. Further improvement to the antenna can be made by transforming the design into a planar antenna which increases the gain from 5.35 dB to 7.73 dB. It is found that doing so increases the return loss bandwidth of the antenna. A study of the substrate size shows that a reduction in size causes the antenna to become narrow band but at the cost of the resonance null depth.

References

[1] A. K. Skrivervik, J. –F. Zurcher, O. Staub, and J. R. Mosig, “PCS antenna design: the challenge of miniaturization,” IEEE Antennas Propag. Mag., 2001, 43, (4), pp. 12-27.

[2] D. Sievenpiper, R. Broas, and E. Yablonovitch, “Antennas on high-impedance ground planes,” IEEE MTTS International Microwave Symposium Digest, 13-19 June 1999, Vol. 3, pp. 1245-1248.

[3] M. E. Ermutlu, C.R. Simovski, M.K. Karkkainen, P. Ikonen, A. A. Sochava, and S.A. Tretyakov, “Patch antennas with new artificial magnetic layers,” arXiv:physics/0504075v1, Apr 2005.

[4] A. P. Feresidis, George Goussetis, S. Wang, and J. C. Vardaxoglou, “Artificial magnetic conductor surfaces and their application to low-profile high-gain planar antennas,” IEEE Trans. Antennas Propag., Vol. 53, no. 1, pp. 209-215, Jan. 2005.

[5] F. Yang, Y. Rahmat-Samii, and A. Kishk, “Low-profile patch-fed surface wave antenna with a monopole-like radiation pattern,” IET Microw. Antennas Propag., Vol. 1, issue 1, pp. 261-266, Feb 2007.

[6] L. Schreider, X. Begaud, M. Soiron, B. Perpere, and C. Renard, “Broadband Archimedean spiral antenna above a loaded electromagnetic bandgap substrate,” IET Microw. Antennas Propag., Vol. 1, issue 1, pp. 212-216, Feb 2007.

[7] A. Erentok, P. L. Luljak, and Richard W. Ziolkowski, “Characterization of a volumetric metamaterial realization of an artificial magnetic conductor for antenna applications,” IEEE Trans. Antennas Propagat., Vol. 53, no. 1, pp. 160-172, Jan. 2005.

[8] C. R. Simovski, M. E, Ermutlu, A. A. Sochava, and S. A. Tretyakov, “Magnetic properties of novel high impedance surfaces,” IET Microw. Antennas Propag., Vol. 1, issue 1, pp. 190-197, Feb 2007.

[9] D. J. Kern, D. H. Werner, A. Monorchio, L. Lanuzza, and M. J. Wilhelm, “The design synthesis of multiband artificial magnetic conductors using high impedance frequency selective surfaces,” IEEE Trans. Antennas Propagat., Vol. 53, no. 1, pp. 8-17, Jan. 2005.

[10] P. Ratajczak, J. -M. Baracco, and P. Brachat, “Adjustable high impedance surface for active reflectarray applications,” Proc. EUCAP, pp. 1-6, 11-16 Nov. 2007.

[11] F. Yang and Y. Rahmat-Samii, “Reflection phase characteristics of the EBG ground plane for low profile wire antenna applications,” IEEE Trans. Antennas Propag., Vol. 51, no. 10, pp. 2691-2703, Oct. 2003.

[12] V. V. S. Prakash and R. Mitra, “Analysis of interaction between microwave antennas and frequency selective surface (FSS) radomes,” IEEE Antennas and Propag. Intl. Symposium, Vol. 4, pp. 404-407, June 2003.

[13] G. I. Kiani, A. R. Wiley, P. Karu, and Esselle, “Frequency Selective Surface Absorber using Resistive Cross-Dipoles,” IEEE Antennas and Propag. Intl. Symposium, pp. 4199-4202, July 2006.

[14] S. Genovesi, R. Mittra, A. Monorchio, and G. Manara, “Particle Swarm Optimization for the Design of Frequency Selective Surfaces,” IEEE Antennas and Propag. Letters, Vol. 5, Issue 1, pp. 277-279, Dec. 2006.

[15] M. Ohira, H. Deguchi, M. Tsuji, and H. Shigesawa, “A singular characteristic of single-layer frequency selective surface with the element optimized by GA,” IEEE Topical Conf. on Wireless Communication Technology, pp. 216-217, Oct. 2003.

[16] M. Hiranandani, A. B. Yakovlev, and A. A. Kishk, “Artificial magnetic conductors realized by frequency selective surfaces on a grounded dielectric slab for antenna applications,” IEE Proc.-Microwave Antennas Propagat. (Part H), Vol. 153, no. 5, pp. 487-493, Oct. 2006.

[17] C. R. Simovski, P. de Maagt, and I. V. Melchakova, “High-impedance surfaces having stable resonance with respect to polarization and incidence angle,” IEEE Trans. Antennas Propagat., Vol. 53, no. 3, pp. 908-914, Mar. 2005.

[18] Y. Zhang, J. von Hagen, M. Younis, C. Fischer, and W. Weisbeck, “Planar artificial magnetic conductors and patch antennas,” IEEE Trans. Antennas Propagat., Vol. 51, no. 10, pp. 2704-2712, Oct. 2003.

[19] G. Goussetis, Y. Guo, A. P. Feresidis, and J. C. Vardaxoglou, “Miniaturized and multiband artificial magnetic conductors and electromagnetic band gap surfaces,” IEEE Antennas Propagat. Society Int. Symp., 20-25 June 2004, Vol. 1, pp. 293-296.

[20] M. Schoeman, U. Jakobas, and B. Woods, “FEKO optimization capabilities: simplex, particle swarm, genetic algorithm,” 2008 ACES Intl. Conference, pp. 281-286, Apr. 2008.

[21] Gopinath Gampala, “Analysis and design of artificial magnetic conductors for X-band antenna applications,” master’s thesis, Univ. of Mississippi, University, 2007.

[22] FEKO Suite 5.4, EM Software and Systems (www.feko.info), 2008.